Convective Instabilities During Directional Solidification

T. D. McCay,* M. H. McCay,† S. A. Lowry,‡ and L. M. Smith§
University of Tennessee Space Institute, Tullahoma, Tennessee

Results of a ground-based experimental program that supports a low-gravity space processing Spacelab experiment are reported. The phenomena which precipitate pluming and thus freckling in a metal alloy are studied in detail using a metal analog (ammonium chloride and water) and the sequential events leading to massive channeling and convection are optically documented. The pluming is shown not to be a random burst of unstable fluid from a preferred channel but, rather, a natural occurrence resulting from a fundamental (Rayleigh-Benard) fluid dynamic instability at the density inversion interface. Rayleigh numbers are calculated for the instability and a critical Rayleigh number is determined.

Nomenclature

A_0 = amplitude of light wave, V/cm^2
B_0 = amplitude of light wave, V/cm^2
D = solutal diffusion coefficient, cm^2/s
d = depth of the inverted layer, cm
f = focal length of lens, cm
g = acceleration of gravity, cm/s^2
h = height of mushy zone, cm
I_i = initial height of mushy zone, cm
j = $\sqrt{-1}$
K_T = thermal diffusivity, cm^2/s
$n(x,y)$ = index of refraction at point (x,y)
R_a = combined Rayleigh number
R_S = solutal Rayleigh number
R_T = thermal Rayleigh number
u_i = image field, V/cm^2
V = solidification rate, cm/s
α_s = solutal coefficient of index of refraction, 1.63×10^{-3}/wt.%
α_T = thermal coefficient of index of refraction, -1.73×10^{-4}/°C
β_s = solutal coefficient of expansion, /wt.%
β_T = thermal coefficient of expansion, /°C
ΔC = concentration change, wt.%
$\Delta\rho$ = density change, gm/cm^3
ΔT = temperature change, °C
η_l = liquid viscosity (poise)
λ = wavelength of light, cm
ϕ = phase of the light wave
τ = distance through the solution, cm
ν = kinematic viscosity, cm^2/s

I. Introduction

DURING the directional solidification of an alloy, a diffusion boundary layer is formed in front of the solidifying interface or growth front. In the case of many superalloys and the metal analog used here, this boundary layer is rich in lighter species and, thus, creates a low density region in front of the interface. For a unidirectional system being solidified in a vertical temperature gradient, the density inversion extends throughout the partially solidified mushy zone, the lightest liquid actually being at the bottom in a conventional casting system. This eventually leads to jets of light material rising through the mushy zone, creating channels or voids and breaking off dendrite arms in the process. These arms are then expelled into the normally supercooled region in front of the interface and can lead to the formation of equiaxed grains that will be trapped within the overall matrix. These grains, which are called freckles, are an undesirable microstructure, as are the channels, both degrading the properties of the final cast material. The study presented here deals with this one aspect of convection within a directionally solidified casting, that is, the formation of interdendritic jets of fluid that generate channels and freckles in the final casting.

II. Background

A. Freckling in Metal Models and Alloys

The ammonium chloride-water system is used as a physical analog for studying the dendritic solidification of metal alloys. For hypoeutectic compositions, ammonium chloride-rich dendrites freeze, rejecting water-rich solution into the surrounding liquid and ahead of the dendrite plus liquid (mushy zone) interface. The rejected solution is less dense than the parent liquid and, therefore, a lighter layer forms creating a density inversion. Since there is an imposed positive temperature gradient, the density of the liquid ahead of the interface appears, as in Fig. 1.

Since the early paper by Jackson and Hunt,[1] two types of criteria have been developed for the freckling phenomena, one primarily based on thermal considerations[2] and the other strictly based on concentration effects.[3] Although these papers recognized the presence of the inverted density layer, explanations of the pertinent phenomena inappropriately used analogies drawn to "salt fingers" and thermosolutal convection. In addition, neither of these two criteria identified the basic fluid instabilities occurring as a result of the inverted layer. The authors recently[4] have extended these early criteria by combining concentration, latent heat, and superposed thermal gradient into an inclusive static stability criteria, but have not attempted to define the responsible fluid instabilities. Experimental work has, however, begun to examine the formation of freckles and their relationship to the inverted layer. Sample and Hellawell demonstrated[5] that perturbation of the portion of the layer ahead of the interface initiated pluming in solidifying ammonium chloride-water solutions. The authors' own

Presented as Paper 88-0258 at the AIAA 26th Aerospace Sciences Meeting, Reno, NV, Jan. 11–14, 1988; received May 9, 1988; revision received Aug. 31, 1988.

*Professor of Engineering Science. Associate Fellow AIAA.
†Associate Professor of Engineering Science. Member AIAA.
‡Graduate Research Assistant. Member AIAA.
§Staff Engineer.

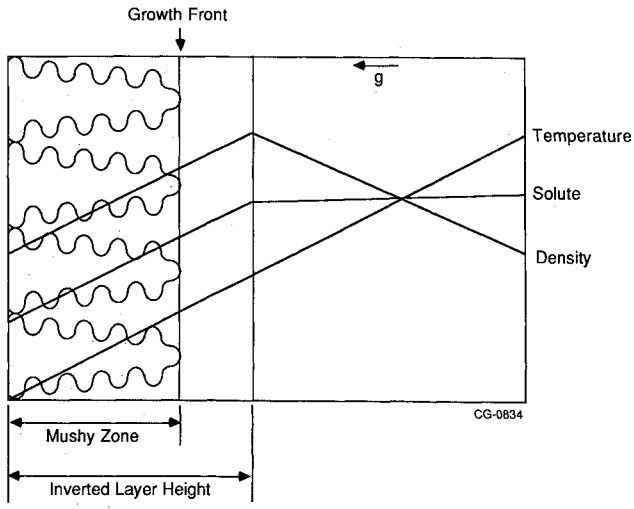

Fig. 1 Schematic of dendrite solidification front with accompanying temperature, solute, and density profiles.

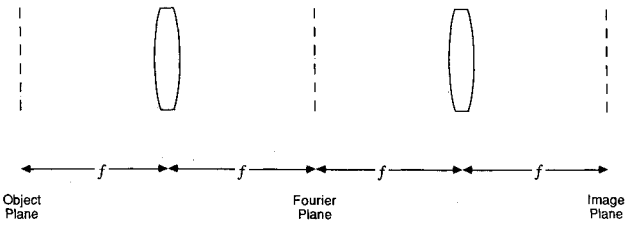

Fig. 2 Confocal optical signal processing system.

experimental work[6] has shown that the inverted layer initially grows proportionally to the interface growth rate, but reaches some maximum thickness prior to pluming, that thickness dictated by fluids phenomena. This paper presents experimental studies conducted to examine the fluid instability that occurs as a result of the density inversion ahead of a dendritic growth front.

B. Optical Data Acquisition Techniques

Because concentration and temperature variations directly affect the index of refraction of the ammonium chloride-water solution, the solidification process can be experimentally studied using techniques of Fourier optics. This approach treats the "optical disturbance" (i.e., the scalar components of the propagating electric or magnetic field) as a two-dimensional signal processed through linear shift-invariant systems.

In passing through the transparent solution, a uniform plane wave traveling in the z direction experiences a multiplicative phase shift, so that the emerging field is described by

$$u_0(x,y) = A_0 e^{j\phi(x,y)} \tag{1}$$

where the phase $\phi(x,y)$ is given by

$$\phi(x,y) = (2\pi\tau/\lambda)n(x,y) \tag{2}$$

In deriving these expressions, it was assumed that the distance through the solution is small enough that the light is not diffracted when traveling from the front to the back surface, and that the index of refraction within the solution does not vary with respect to z, the direction of propagation of the light. Because any practical detector responds to the intensity of the radiation, direct imaging of the field emerging from the solution yields no useful information about the phase. Thus, the problem is how to process the light to extract the phase information in terms of variations in intensity in the resulting image.

The method chosen to accomplish this employs a confocal optical signal processing system, as shown in Fig. 2. Two lenses, each with focal length f, are centered on the optical axis at a distance $2f$ apart. In this way, an object in the front focal plane of the first lens is imaged at unity magnification onto the back focal plane of the second lens. The field in the back focal plane of the first lens is proportional to the Fourier transform of the field in the front focal plane. This arrangement allows for direct frequency domain filtering of the object field by placing appropriate spatial filters in the Fourier plane.

C. Thermosolutal Instabilities

Thermosolutal instabilities in solidifying systems have been a significant research subject for several years[7] and are considered the principal culprit in freckle formation. They are discussed here for completeness but, although they do drive flows in these systems, they are not the primary cause of the initial instabilities. Most alloys are not solidified using a sufficiently steep temperature gradient to dictate a statically stable density profile, the classic condition associated with thermosolutal instability. A thorough discussion of thermosolutal instabilities is given by Linden.[8] He identifies two categories, finger instability and diffusive convective instability. In the finger instability, one normally has a stabilizing temperature gradient (temperature decreases with depth) and a destabilizing concentration gradient (lighter component increases with depth), but the temperature gradient overpowers the concentration gradient and the density continuously increases with depth. If the thermal diffusivity exceeds the mass diffusivity, this situation is dynamically unstable. Consider a parcel of fluid perturbed downwards, for example. It is thermally buoyant but solutally negatively buoyant. It would be prone to rise back to its equilibrium position, except that on its journey it loses heat at one rate and gains solute at a different, slower rate, thus gaining negative buoyancy. This will continue, since the two gradients continue to exist and the parcel will continue to sink. The same type of argument holds for a parcel displayed upwards, it will continue to rise. This phenomena, the finger instability, was discovered over 30 years ago by oceanographers[9] and was given the name salt fingers—cool columns of water rising, surrounded by warm falling columns of salty water.

The other instability corresponds to the opposite case, in which the fast diffusing component (heat) is destabilizing. This situation leads to an overstable oscillation.

D. Classic Rayleigh-Benard Instabilities

Classic Rayleigh-Benard (R-B) instabilities include convective rolls for the case where the fluid has contact with a solid surface at both horizontal boundaries and Benard cells when the upper boundary is free. An excellent review of these phenomena can be found in several articles in the collection edited by Zierep and Oertel.[10] The R-B instabilities differ from those discussed in the previous section in that thermal gradients alone are considered. For such cases, the thermal Rayleigh number can be defined as

$$R_T = \frac{g\beta_T d^3 \Delta T}{\nu K_T} \tag{3}$$

The stability of the solidifying ammonium chloride system being studied here can be examined in an analogous fashion with the additional definition of a solutal Rayleigh number

$$R_s = \frac{g\beta_s d^3 \Delta C}{\nu D} \tag{4}$$

If the instability that occurs for the ammonium chloride-water system is a classic R-B instability, it should be possible to

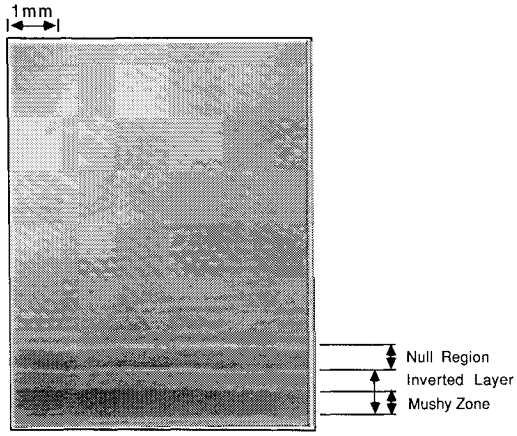

Fig. 3 The growth front of directionally solidified ammonium chloride-water at breakdown as shown by a confocal optical signal processing system.

establish the stability boundaries based on a Rayleigh number, represented by a combination of thermal and solutal

$$R_A = R_T + R_s \tag{5}$$

III. Experimental Techniques and Procedures

A. The Solidification System

The directional solidification system was similar to that used previously.[6] It consisted of a sealed quartz cuvette (25 × 16 × 12 mm) that contained the ammonium chloride-72% water solution, and two thermoelectric devices (TED) that provided the required top and bottom temperatures on the 16 × 12 mm surfaces. Optical measurements were made through the 25 × 16 mm surfaces. The temperature profiles and cooling rates were controlled by an IBM Compatible PC-XT computer with a Keithley multiplexing system. Temperatures were monitored optically with fringe spacing measurements and by chromel-alumel thermocouples at the interfaces between the TED's and the cuvette.

B. The Optical System

Several techniques for processing phase images using a confocal optical signal processing system are discussed in Goodman.[11] In the technique used here, called the *central dark ground* method, a field such as that given in Eq. (1) is present in the object plane.

If a small opaque obstruction is placed at the origin in the Fourier plane, the low spatial frequency components are effectively removed, and the resulting image field is approximately given by

$$u_i(x,y) = A_0 e^{j\phi(x,y)} - B_0 \tag{6}$$

where B_0 denotes the low-frequency components of the field that can be approximated by a constant. The intensity in the image plane is, therefore,

$$I_i(x,y) = A_0^2 + B_0^2 - 2A_0B_0\cos[\phi(x,y)] \tag{7}$$

Thus, the phase induces systematic variations in the image intensity. The system produces data similar to an interferometer but is considerably simpler and more rugged.

In the experiment discussed here, phase and, thus, intensity variations are driven by changes in the index of refraction. The dependence of the ammonium chloride-water index of refraction on temperature and concentration and can be given by[12]

$$n = 1.3822 + \alpha_T(T - 22°\text{C}) + \alpha_s(C - 27.07\ \text{wt.\%}) \tag{8}$$

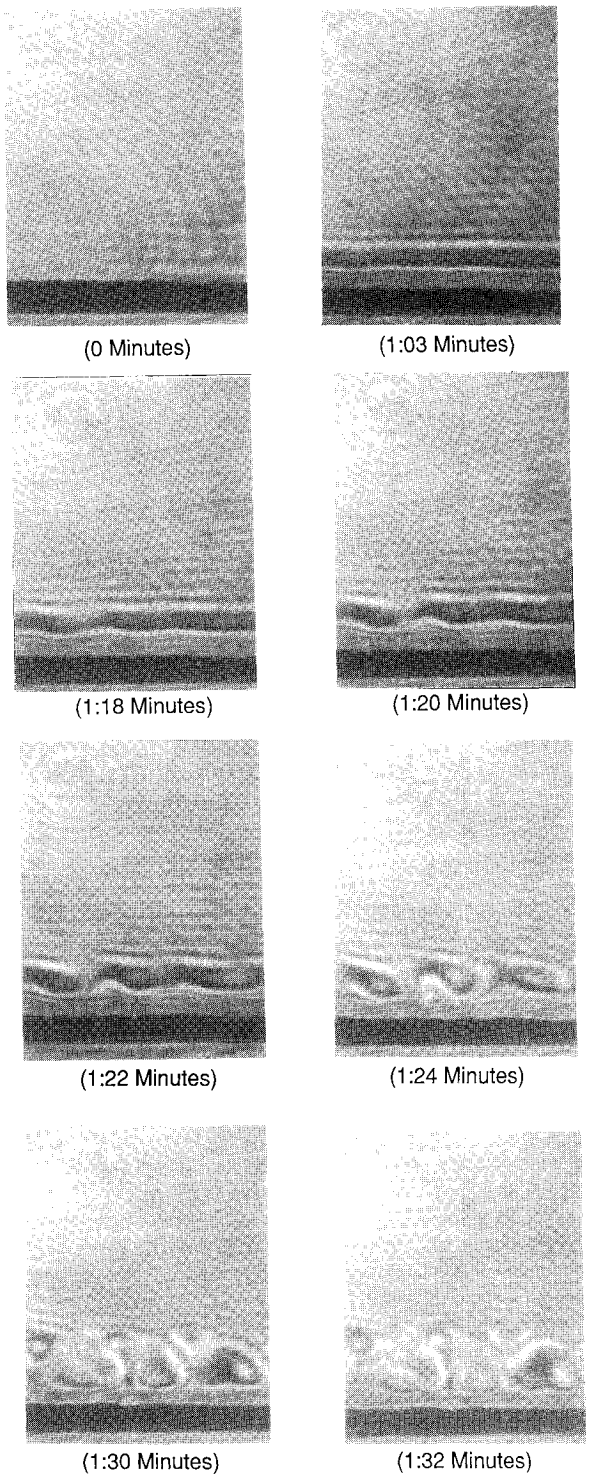

Fig. 4 Inverted layer growth and breakdown during directional solidification of NH_4Cl-H_2O.

During directional solidification of ammonium chloride-water, the index of refraction goes through a reversal similar to the density. The reversal for density and index of refraction occur at the same location if

$$(\alpha_T/\alpha_s)/(\beta_T/\beta_s) = 1 \tag{9}$$

In the case of ammonium chloride-water, the experimentally determined[13] value of the quantity is 1.014, and for the purposes of this analysis the density inversion is considered to be at the same position in the liquid as the index of refraction inversion.

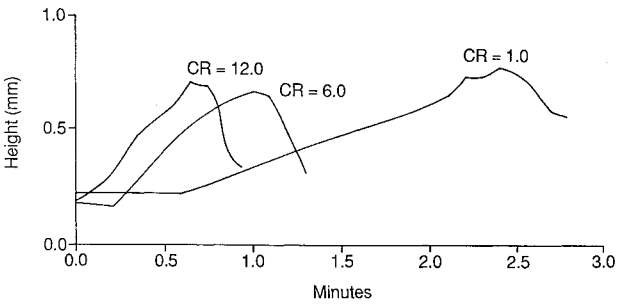

Fig. 5 The height of the inverted layer as a function of time for three cooling rates (°C/min) and a temperature gradient of 28°C/cm.

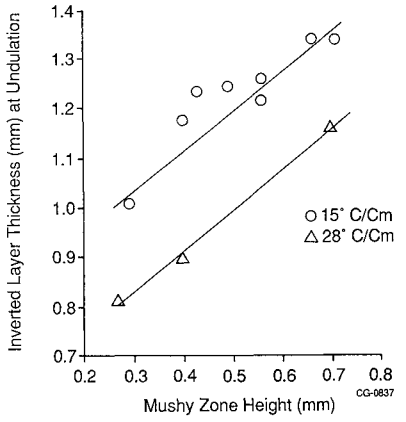

Fig. 6 Inverted layer thickness at undulation as a function of mushy zone height for two gradients and a cooling rate of 2°C/min.

C. The Image Processor

The image intensity data were acquired by placing the light-sensitive detector of a video camera in the image plane; the confocal optical system simply replaces the standard lens usually mounted on the video camera. Data were then recorded in real time in video format and stored on magnetic tape. Quantitative information was obtained by first digitizing selected video frames into 512 × 512-pixel image format, and then visually selecting the layer and growth front height with the aid of a cursor. Spatial dimensions within the digital image were measured by calibrating the entire data acquisition system to determine vertical and horizontal pixel spacing.

D. Experimental Procedure

The solidification sequence consisted of preheating the cuvette and solution to a temperature above 40°C for 10 min. The desired temperature gradient was then superposed across the cuvette with a holding time of several hours to ensure homogeneity in the solution and establish a starting mushy zone height. The top and bottom TED's were then ramped down at selected cooling rates while maintaining the constant temperature gradient. A matrix of experiments was conducted in which initial mushy zone height was varied from 0.02–0.09 mm and the cooling rate was varied from 0.1–12.0°C/min. Temperature gradients of 15°C/cm and 28°C/cm were investigated. The solidification rate (cm/h) during this time period of the experiment was a factor of 0.275 times the cooling rate (°C/min). Video recording of the image was taken real time, beginning with the onset of the cooling ramp. A typical confocal optical signal processing central dark ground image is given in Fig. 3. The visible portion of the inverted layer is clearly indicated by the bright area just above the mushy zone. The edge of the inverted layer was taken to be that point at which the bright layer began to fade into the

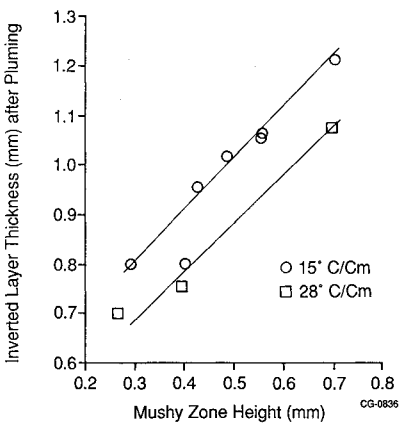

Fig. 7 Inverted layer thickness after pluming as a function of mushy zone height for two gradients and a cooling rate of 2°C/min.

black region (null) above it. Using both manual and digital image analysis techniques, the height of the layer above the bottom of the mushy zone was measured as a function of time for each initial mushy zone height, and the onset of layer breakdown and pluming was noted.

IV. Experimental Observations

A. Inverted Layer Build-up and Breakdown

Figure 4 shows the mushy zone and inverted layer as a function of time after the initiation of cooling. The sequence of events are as follows:

1) A mushy zone exists in a stable temperature gradient.
2) Cooling is initiated (time = 0) and growth begins.
3) A dark (null) band forms ahead of the mushy zone.
4) A bright band, the leading portion of the inverted layer, begins to form ahead of the mushy zone.
5) The inverted layer grows in height with the dark band moving ahead of it.
6) Fringes appear within the growing inverted layer.
7) Periodic undulations occur along the top of the inverted layer.
8) Periodic undulations occur along the top of the dark band.
9) Periodic rolls appear within the dark band.
10) Plumes of liquid rise between some of the rolls, breaking up their periodicity.
11) The inverted layer retreats.
12) Individual dendrites rapidly grow out from the mushy zone and extend past the inverted layer.
13) Erratic pluming and rapid growth of the entire front ensues.

B. Quantitative Measurements

The mushy zone height and inverted layer thickness were measured as functions of time for three growth rates. The growth with time of the inverted layer thickness is shown in Fig. 5. The inverted layer thickness at the onset of event number 8 when the periodic undulations began to occur, and during event number 12, when it retreated, is given in Figs. 6 and 7 as a function of mushy zone height (at undulation), at a constant cooling rate for the two temperature gradients.

V. Discussion

The event sequence listed in Sec. IV has been consistent for all conditions studied. The condition variables were initial mushy zone height, cooling rate, and temperature gradient.

Using the same event numbering assigned in the previous section, the following explanations are offered:

1) and 2) Self-explanatory.

3) For the confocal optical arrangement, a null is expected for a region of constant index of refraction. The signs

on α_T and α_s indicate that an inflection in n (null) must occur for positive gradients in both temperature and salt. This is the case in the diffusion boundary layer, and the null represents the extent of that region. Examining the variation of density (β_T and β_s), one concludes that below the null there exists an increasing (with height) density gradient and above the null a decreasing one.

4) The next step after the null would be the change of optical phase, giving a light band for the steepening concentration gradient. As the layer grows, successive fringes appear.

5) and 6) Continuation of event number 4.

7) This phenomena was not anticipated. Generally, it is thought that pluming begins in a random fashion and the layer should break down in that manner. Instead, a periodic undulation of the top of the layer began first. This undulation is more consistent with linear stability theory associated with R-B type systems. The height at which this occurred was a function of the initial mushy zone height and was reasonably consistent over the range of parameters investigated.

8) A consequence of event number 7.

9) These undulations develop into regions with optical depth changes that provide a roll appearance. Preliminary particle studies[13] indicate that these rolls are actually Benard cells rather than periodic starting plumes.

10) At some later time (function of cooling rate and thermal gradient) pluming did begin. The plume was always located between two of the rolls, apparently consisting of buoyant fluid from within the mushy zone.

11) This appears to be the *draining of the swamp* discussed by Hellawell.[5] The pluming material now resembles a salt finger system and the flow is supplied by fluid from throughout the inverted layer region. The portion of the layer ahead of the interface seems to be stable, i.e., the visible layer moves down uniformly. This height is maintained for a considerable time period.

12) and 13) The fresh solute from the convection makes this possible. Once the dendrites move into the fresh fluid, rapid growth (not diffusion limited) can proceed and the growth rate approaches the cooling rate.

The growth of the inverted layer as a function of time is depicted in Fig. 5. For each rate, the layer reaches a maximum height and then decreases with time. The peaks of the curves correspond to the time of undulation.[6] The drop-off occurs subsequently to pluming.

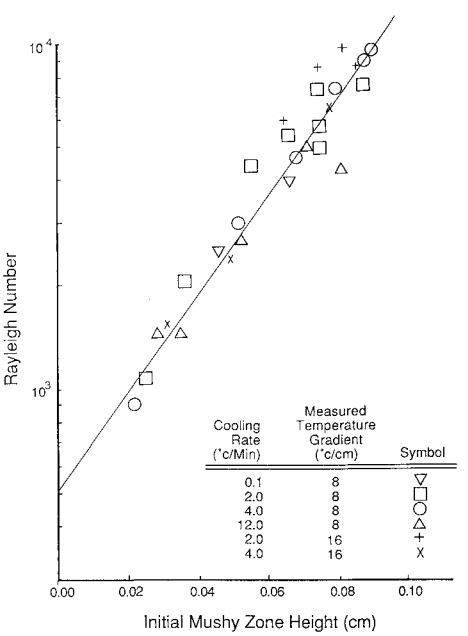

Fig. 8 Critical Rayleigh number variation with initial height of the mushy zone.

The inverted layer thickness (at undulation) with mushy zone height is seen to be directly proportional in Fig. 6. These data were obtained by starting the growth at various initial mushy zone heights. If one begins with a larger initial thickness, then an increased inverted layer thickness is reached before undulation begins. The stability of the layer can be examined in the case of an R-B instability by employing Eq. (5). The Rayleigh number at undulation should correspond to a critical value. Since the inverted layer thickness at breakdown increases with initial mushy zone height, the critical Rayleigh number will also. The explanation for this behavior lies in the frictional effects dictated by the mushy zone, which acts as a porous mesh. The mushy zone increases the effective viscosity, thereby giving a lower effective Rayleigh number than one would calculate from Eq. (5). Figure 8 gives the breakdown Rayleigh number as a function of initial mushy zone height for several different conditions. The effective or actual critical Rayleigh number can be estimated by determining the value that would exist if the initial mushy zone thickness was zero. This gives a value of approximately 600, which compares favorably with a critical solutal Rayleigh number of 1000, reported in earlier literature.[14] Based upon Fig. 8, it can be concluded that the effective viscosity increases with mushy zone height in an exponential manner.

VI. Conclusions

Based upon the work presented, several conclusions can be drawn:

1) The phenomena associated with freckling in metal alloys can be successfully studied using ammonium chloride-water solutions.

2) The confocal optical signal processing arrangement serves very well as the poor man's interferometer. It is more rugged and considerably simpler.

3) The well-behaved phenomena of undulations and subsequent cell formation preceding pluming is not consistent with a thermosolutal instability. Thus, many of the defects in castings of superalloys (which behave similarly to ammonium chloride-water) may be inappropriately attributed to thermosolutal effects. A detailed evaluation of the Lewis number for each specific system is necessary to answer that question fully.

4) The breakdown behavior that leads to pluming appears to be a solutal analogy to the classic Rayleigh-Benard instability. A critical Rayleigh number that is dependent upon the initial mushy zone height can be determined for the system. For ammonium chloride-water, the critical Rayleigh number is approximately 600.

Acknowledgment

This work was sponsored by NASA under Contract 8-37292. Mr. Rudy Ruff of NASA Marshall Space Flight Center is the technical monitor.

References

[1]Jackson, K. A. and Hunt, J. D., "Transparent Compounds that Freeze Like Metals," *Acta Metallurgica*, Vol. 13, May 1965, pp. 1212–1215.

[2]Copley, S. M., Giamei, A. F., Johnson, S. M., and Hornbecker, M. R., "The Origin of Freckles in Unidirectionally Solidified Castings," *Metallurgica Transactions*, Vol. 1, Aug. 1970, pp. 2193–2204.

[3]Sharp, R. M. and Hellawell, A., "The Incidence of Convection During Solidification," *Journal of Crystal Growth*, Vol. 12, Oct. 1972, pp. 261–262.

[4]McCay, T. D. and McCay, M. H., "An Inclusive Static Stability Criteria for Freckling in Directional Solidification of Metal Models and Alloys," *Acta Metallurgica* (submitted for publication).

[5]Sample, A. K. and Hellawell, A., "The Mechanism of Formation and Prevention of Channel Segregation During Alloy Solidification," *Metallurgica Transactions*, Vol. 15A, Dec. 1984, pp. 2163–2173.

[6]McCay, M. H. and McCay, T. D., "Experimental Measurement of Solutal Layers in Unidirectional Solidification," *Journal of Thermophysics and Heat Transfer*, Vol. 2, No. 3, July 1988, pp. 197–202.

[7]Coriell, S. F., Cordes, M. R., Boettinger, W. J., and Sekerka, R. F., "Convective and Interfacial Instabilities During Unidirectional Solidification of a Binary Alloy," *Journal of Crystal Growth*, Vol. 49, May 1980, pp. 13–28.

[8]Linden, P. F., "Diffusive Instabilities and Porous Media," *Convective Transport and Instability Phenomena*, edited by J. Zierep and H. Oertel Jr., G. Braun, Karlsruhe, Federal Republic of Germany, 1982, pp. 171–199.

[9]Stommel, H., Arous, A. B., and Blanchard, D., "An Oceanographical Curiosity: The Perpetual Salt Fountain," *Deep-Sea Research*, Vol. 3, April 1956, pp. 152–153.

[10]*Convective Transport and Instability Phenomena*, edited by J. Zierep and H. Oertel Jr., G. Braun, Karlsruhe, Federal Republic of Germany, 1982.

[11]Goodman, J. W., *Introduction to Fourier Optics*, McGraw-Hill, San Francisco, CA, 1968, pp. 141–197.

[12]Johnston, M. H., Owen, R. B., and Shurney, R. E., "Optical Observations of Unidirectional Solidification in Microgravity," NASA TP-2110, Jan. 1983.

[13]Gray, P. A., "Experimental Study of Convective Breakdown in Solidification of a Metal Model Material," M.S. Thesis, Univ. of Tennessee Space Inst., Tullahoma, TN, Dec. 1988.

[14]Grodzka, P. G., "Types of Natural Convection in Space Manufacturing Processes: Summary Report, Lockheed Missiles and Space Company, Inc., Huntsville Research Park, Huntsville, AL, NAS8-25577, LMSC-HREC TR D306350, Jan. 1973.